Study of Air Fuel Ratio and Instantaneous Behaviour on Crank Angle of Four Cylinder Direct Injection Hydrogen Fueled Engine

M. M. Rahman, *Member, IAENG*, Mohammed K. Mohammed, Rosli A. Bakar and M.S.M. Sani, *Member, IAENG*

Abstract— **The present study focuses on the effect of air-fuel ratio and instantaneous behaviour on crank angle of four cylinder direct injection hydrogen fueled engine. GT-Power was utilized to develop the model for direct injection engine. Air-fuel ratio was varied from rich limit (AFR=27.464) to a lean limit (AFR=171.65). The rotational speed of the engine was varied from 2500 to 4500 rpm. It can be seen from the obtained results that the air fuel ratio are greatly influence on the brake mean effective pressure (BMEP), brake efficiency (BE), brake specific fuel consumption (BSFC) as well as the maximum cylinder temperature. It can be seen that the decreases of BMEP, BE and maximum cylinder temperature with increases of air fuel ratio and speed, however, increases the brake specific fuel consumption. For rich mixtures (low AFR), BMEP decreases almost linearly, then BMEP falls with a non-linear behavior. It can be observed that the brake thermal efficiency is increases nearby the richest condition (AFR ≅ 35) and then decreases with increases of air fuel ratio. Maximum η_b of 35.4% at speed 2500 rpm can be seen compared with 26.3% at speed 4500 rpm. The optimum minimum value of BSFC occurred within a range of AFR from 38.144 ($\theta = 0.9$) to 49.0428 ($\theta = 0.7$) for the selected range of speed. The effect of the rotational speed on the instantaneous behavior of the cylinder pressure is no significant. The flame development, propagation and termination period consumes about 5% and 90% of the air fuel mixture and finally flame termination period which consumes about the rest of the mixture (5%). The present contribution suggests the direct injection fuel supply system as a strong candidate for solving the power and abnormal combustion problems.**

***Index Terms*— hydrogen fueled engine, direct injection, air fuel ratio, engine performance, crank angle, rotational speed.**

Manuscript received August 10, 2008. This work was supported by the Universiti Malaysia Pahang.

M. M. Rahman is with the Faculty of Mechanical Engineering, Universiti Malaysia Pahang, Tun Abdul Razak Highway, 26300 Gambang, Kuantan, Pahang, Malaysia (phone: 609-5492207; fax: 609-5492244; e-mail: mustafizur@ump.edu.my).

Mohammed K. Mohammed is with the Faculty of Mechanical Engineering, Universiti Malaysia Pahang, Tun Abdul Razak Highway, 26300 Gambang, Kuantan, Pahang, Malaysia.

Rosli A. Bakar is with the Faculty of Mechanical Engineering, Universiti Malaysia Pahang, Tun Abdul Razak Highway, 26300 Gambang, Kuantan, Pahang, Malaysia

M.S.M. Sani is with the Faculty of Mechanical Engineering, Universiti Malaysia Pahang, Tun Abdul Razak Highway, 26300 Gambang, Kuantan, Pahang, Malaysia

I. Introduction

The status of the availability of the fossil fuels is critical and the prices have been jumped to levels that never been reached before. Furthermore, the environmental problems are serious and the politics all over the world applied severe conditions for the automotive industry. Researchers, technologists and the automobile manufacturers are increasing their efforts in the implementation of technologies that might be replaced fossil fuels as a means of fueling existing vehicles. Hydrogen, as alternative fuel, has unique properties give it significant advantage over other types of fuel. However, the widespread implementation of hydrogen for vehicular application is still waiting several obstacles to be solved. These obstacles are standing in the production, transpiration, storage and utilization of hydrogen. The most important one is the utilization problems. Hydrogen induction techniques play a very dominant and sensitive role in determining the performance characteristics of the hydrogen fueled internal combustion engine (H_2ICE) [1]. Hydrogen fuel delivery system can be broken down into three main types including the carbureted injection, port injection and direct injection [2].

In direct injection, the intake valve is closed when the fuel is injected into the combustion cylinder during the compression stroke [2]. Like PFI, direct injection has long been viewed as one of the most attractive choices for supplying hydrogen fuel to combustion chamber [3-5]. This view is based on: its prevention for abnormal combustion: pre-ignition, backfire and knock; and the high volumetric efficiency, (since hydrogen is injected after intake valve closing). The improved volumetric efficiency and the higher heat of combustion of hydrogen compared to gasoline, provides the potential for power density to be approximately 115% that of the identical engine operated on gasoline [3]. However, it is worthy to emphasize that while direct injection solves the problem of pre-ignition in the intake manifold, it does not necessarily prevent pre-ignition within the combustion chamber [2]. Metal hydrides can only provide low pressure hydrogen, compressed hydrogen could be used but this limits the effective tank contents as the tank can only be emptied down to the fuel injection pressure. Compressing gaseous hydrogen on board would mean an extra compressor and a substantial energy demand [6]. The high pressure was defined by White et al. [3] as greater than 80 bar to ensure sonic injection velocities and high enough mass flow rates for start of injection throughout the compression stroke. The

need for rapid mixing necessitates the use of critical flow injectors and the short time duration with late injection requires high mass flow rates. The valve leakage at the valve seat and the losses associated with the injection system are another issues [7-8]. Another important challenge for DI is the extremely short time for hydrogen–air mixing. For early injection (i.e., coincident with inlet valve closure (IVC)) maximum available mixing times range from approximately 20–4 ms across the speed range 1000–5000 rpm, respectively [3]. This insufficient time leads to unstable engine operation at low hydrogen-air equivalence ratios due to insufficient mixing between hydrogen and air [9]. Late injection, as a solution, was investigated by Mohammadi et al. [4]. However, this measure is insufficient and the system will be susceptible for pre-ignition as stated above. Therefore, additional transactions like utilization of other techniques such as EGR and after-treatment methods are required to bring the NOx emission to acceptable level [4]. The present contribution introduces a model for a four cylinders, direct injection H2ICE. GT-Power software code is used to build this model. The objectives of this study are to investigate the effect of air fuel ratio on the engine performance and instantaneous behaviour of intake, exhaust port pressure and cylinder pressure on the crank angle of the direct inject engine.

II. Hydrogen Engine Model

A. Engine Performance Parameters

The brake mean effective pressure (*BMEP*) can be defined as the ratio of the brake work per cycle W_b to the cylinder volume displaced per cycle V_d, and it can be expressed as in (1).

$$\mathrm{BMEP} = \frac{W_b}{V_d} \tag{1}$$

Equation (1) can be rewrite for the four stroke engine as in (2).

$$\mathrm{BMEP} = \frac{2P_b}{NV_d} \tag{2}$$

where P_b is the brake power, and N is the rotational speed.

Brake efficiency (η_b) can be defined as the ratio of the brake power P_b to the engine fuel energy as in (3):

$$\eta_b = \frac{P_b}{\dot{m}_f (LHV)} \tag{3}$$

where $\dot{m}_f$ is the fuel mass flow rate and *LHV* is the lower heating value of hydrogen.

The brake specific fuel consumption (*BSFC*) represents the fuel flow rate $\dot{m}_f$ per unit brake power output and can be expressed as in (4):

$$BSFC = \frac{\dot{m}_f}{P_b} \tag{4}$$

The volumetric efficiency (η_v) of the engine defines as the mass of air supplied through the intake valve during the intake period ($\dot{m}_a$) by comparison with a reference mass, which is that mass required to perfectly fill the swept volume under the prevailing atmospheric conditions, and can be expressed as in (5):

$$\eta_v = \frac{\dot{m}_a}{\rho_{ai} V_d} \tag{5}$$

where ρ_{ai} is the inlet air density.

B. Engine Model

The engine model for an in-line 4-cylinder direct injection engine was developed for this study. Engine specifications for the base engine are tabulated in Table 1. The specific values of input parameters including the AFR, engine speed, and injection timing were defined in the model. The boundary condition of the intake air was defined first in the entrance of the engine. The air enters through a bell-mouth orifice to the pipe. The discharge coefficients of the bell-mouth orifice were set to 1 to ensure the smooth transition as in the real engine. The pipe of bell-mouth orifice with 0.07 m of diameter and 0.1 m of length are used in this model. The pipe connects in the intake to the air cleaner with 0.16 m of diameter and 0.25 m of length was modeled. The air cleaner pipe identical to the bell-mouth orifice connects to the manifold. A log style manifold was developed from a series of pipes and flow-splits. The intake system of the present study model is shown in Fig. 1. The total volume for each flow-split was 256 cm^3. The flow-splits compose from an intake and two discharges. The intake draws air from the preceding flow-split. One discharge supplies air to adjacent intake runner and the other supplies air to the next flow-split. The last discharge pipe was closed with a cup to prevent any flow through it because there is no more flow-split. The flow-splits are connected with each other via pipes with 0.09 m diameter and 0.92 m length. The junctions between the flow-splits and the intake runners were modeled with bell-mouth orifices. The discharge coefficients were also set to 1 to assure smooth transition, because in most manifolds the transition from the manifold to the runners is very smooth. The intake runners for the four cylinders were modeled as four identical pipes with .04 m diameter and 0.1 m length. Finally the intake runners were linked to the intake ports which were modeled as pipes with 0.04 m diameter and 0.08 length. The air mass flow rate in e intake port was used for hydrogen flow rate based on the imposed AFR.

Table1: Engine specification

Engine Parameter	Value	Unit
Bore	100	mm
Stroke	100	mm
Connecting rod length	220	mm
Piston pin offset	1.00	mm
Total displacement	3142	(cm^3)
Compression ratio	9.5	
Inlet valve close, IVC	-96	^{0}CA
Exhaust valve open, EVO	125	^{0}CA
Inlet valve open, IVO	351	^{0}CA
Exhaust valve close, EVC	398	^{0}CA

The second major part of the engine model is the powertrain model which is shown in Fig. 2. In the powertrain, the induced air passes through the intake cam-driven type valves with 45.5 mm of diameter to the cylinders. The valve lash

(mechanical clearance between the cam lobe and the valve stem) was set to 0.1 mm. The overall temperature of the head, piston and cylinder for the engine parts are listed in Table 2. The temperature of the piston is higher than the cylinder head and cylinder block wall temperature because this part is not directly cooled by the cooling liquid or oil.

Table 2: Temperature of the mail engine parts

Components	Temperature (K)
Cylinder head	550
Cylinder block wall	450
Piston	590

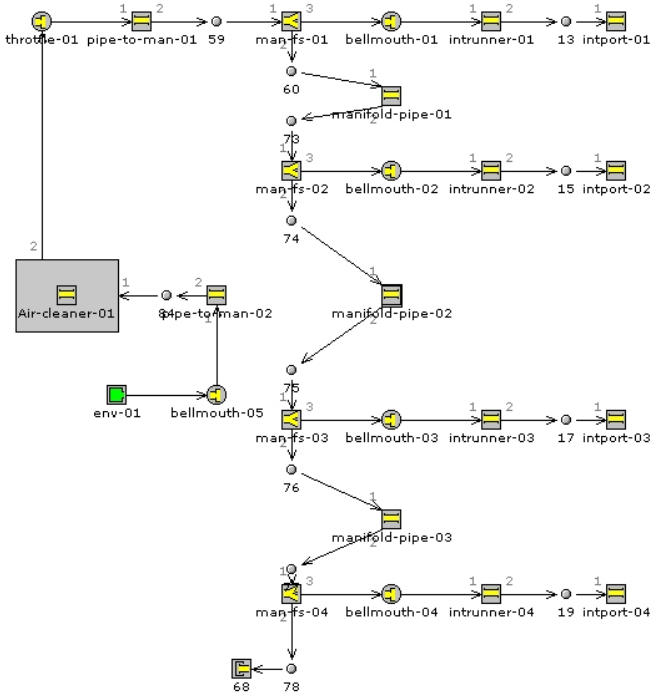

Fig. 1. Intake system model

The last major part in the present model is the exhaust system which is shown in Fig. 3. The exhaust runners were modeled as rounded pipes with 0.03 m inlet diameter, and 80^0 bending angle for runners 1 and 4; and 40^0 bending angle of runners 2 and 3. Runners 1 and 4, and runners 2 and 3 are connected before enter in a flow-split with 169.646 cm^3 volume. Conservation of momentum is solved in 3-dimentional flow-splits even though the flow in GT-Power is otherwise based on a one-dimensional version of the Navier-Stokes equation. Finally a pipe with 0.06 m diameter and 0.15 m length connects the last flow-split to the environment. Exhaust system walls temperature was calculated using a model embodied in each pipe and flow-split. Table 3 are listed the parameters used in the exhaust environment of the model.

Table 3. Parameters used in the exhaust environment

Parameters	Value	Unit
External environment temperature	320	K
Heat transfer coefficient	15	W/m^2K
Radiative temperature	320	K
Wall layer material	Steel	
Layer thickness	3	mm
Emissivity	0.8	

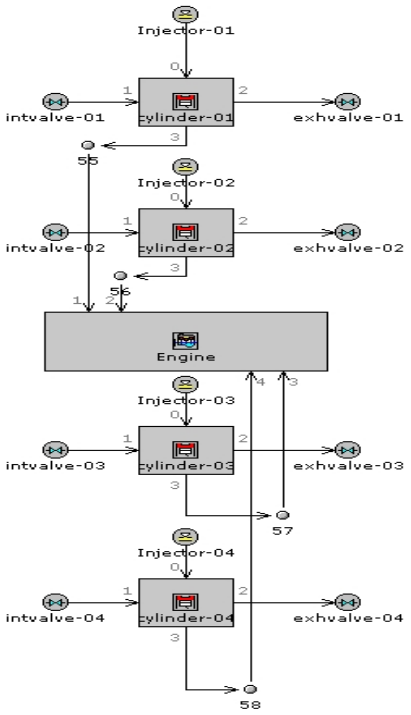

Fig. 2. Powertrain model

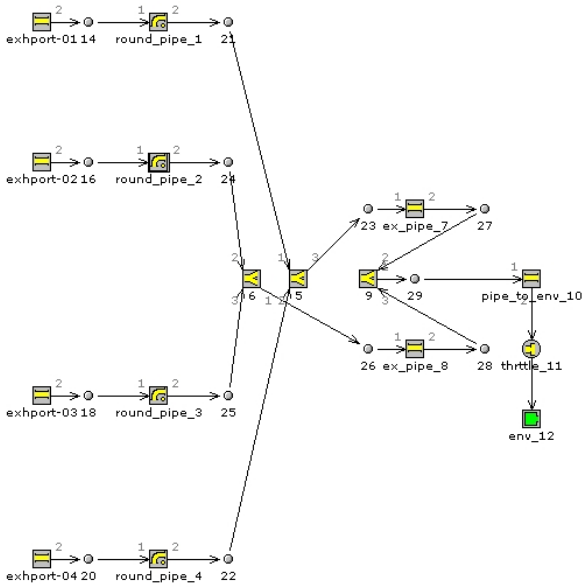

Fig. 3. Exhaust system model

III. Results and Discussion

A lean mixture is one in which the amount of fuel is less than stoichiometric mixture. This leads to fairly easy to get an engine start. Furthermore, the combustion reaction will be more complete. Additionally, the final combustion temperature is lower reducing the amount of pollutants. Figure 4 shows the effect of air-fuel ratio on the brake mean effective pressure. The air-fuel ratio AFR was varied from rich limit (AFR = 27.464:1 based on mass where the equivalence ratio (ϕ = 1.2) to a very lean limit (AFR =171.65 where ϕ = 0.2) and engine speed varied from 2500 rpm to 4500 rpm. *BMEP* is a good parameter for

comparing engines with regard to design due to its independent on the engine size and speed.

A. Effect of Air Fuel Ratio on Engine Performance

It can be seen that *BMEP* decreases with increases of *AFR* and speed. This decrease happens with two different behaviors. For rich mixtures (low AFR), *BMEF* decreases almost linearly, then *BMEP* falls with a non-linear behavior. Higher linear range can be recognized for higher speeds. For 4500 rpm, the linear range is continuing until AFR of 42.9125 (ϕ =0.8). The non-linear region becomes more predominant at lower speeds and the linear region cannot be specified there. The total drop of *BMEP* within the studied range of AFR was 8.08 bar for 4500 rpm compared with 10.91 bar for 2500 rpm. At lean operating conditions (AFR = 171.65, ϕ =0.2 the engine gives maximum power (*BMEP* = 1.635 bar) at lower speed 2500 rpm) compared with the power (*BMEP* = 0.24 bar) at speed 4500 rpm. Due to dissociation at high temperatures following combustion, molecular oxygen is present in the burned gases under stoichiometric conditions. Thus some additional fuel can be added and partially burned. This increases the temperature and the number of moles of the burned gases in the cylinder. These effects increases the pressure were given increase power and mean effective pressure.

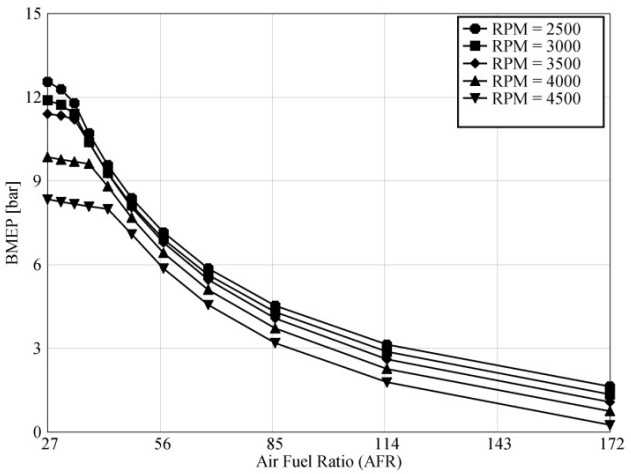

Fig. 4 Variation of brake mean effective pressure with air fuel ratio for various engine speeds

Figure 5 shows the variation of the brake thermal efficiency with the air fuel ratio for the selected speeds. Brake power is the useful part as a percentage from the intake fuel energy. The fuel energy is also covered the friction losses and heat losses (heat loss to surroundings, exhaust, enthalpy and coolant load). Therefore lower values of η_b can be seen in Fig. 5. It can be observed that the brake thermal efficiency is increases nearby the richest condition (AFR ≅ 35) and then decreases with increases of AFR and speed. The operation within a range of AFR from 38.144 to 42.91250 (ϕ = 0.9 to 0.8) gives the maximum values for η_b for all speeds. Maximum η_b of 35.4% at speed 2500 rpm can be seen compared with 26.3% at speed 4500 rpm. Unaccepted efficiency η_b of 3.7% can be seen at very lean conditions with AFR of 171.65 (ϕ =0.2 for speed of 4500 rpm while a value of 23.86% was recorded at the same conditions with speed of 2500 rpm. Clearly, rotational speed has a major effect in the behavior of η_b with AFR. Higher speeds lead to higher friction losses.

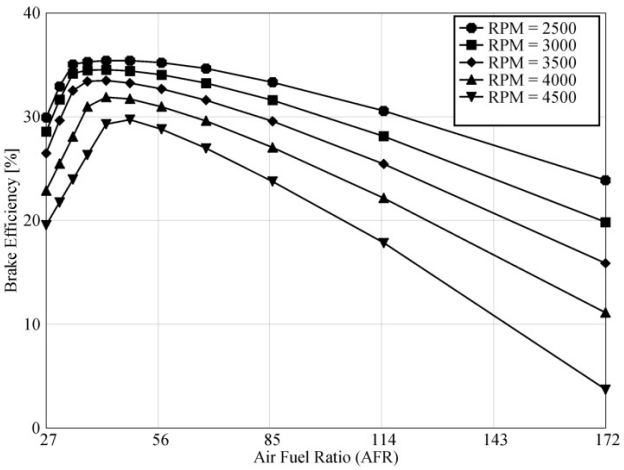

Fig. 5. Variation of brake thermal efficiency with air fuel ratio

Figure 6 depicts the behavior of the brake specific fuel consumption *BSFC* with AFR. It is clearly seen that the higher fuel is consumed at higher speeds due to the greater friction losses that can occur at high speeds. It is easy to perceive from the figure that there is an optimum minimum value of *BSFC* occurred within a range of AFR from 38.144 (ϕ =0.9) to 49.0428 (ϕ =0.7) for the selected range of speed. At very lean conditions, higher fuel consumption can be noticed. After AFR of 114.433 (ϕ =0.3) the *BSFC* rises up rapidly, especially for high speeds. At very lean conditions with AFR of 171.65 (ϕ =0.2), a *BSFC* of 125.87 *g/kW-h* was observed for the speed of 2500 rpm; while it was 809 *g/kW-h* for 4500 rpm. The value *BSFC* at speed of 2500 rpm was doubled around 2 times at speed of 4000 rpm; however the same value was doubled around 5 times at speed of 4500 rpm. This is because of very lean operation conditions can lead to unstable combustion and more lost power due to a reduction in the volumetric heating value of the air/hydrogen mixture.

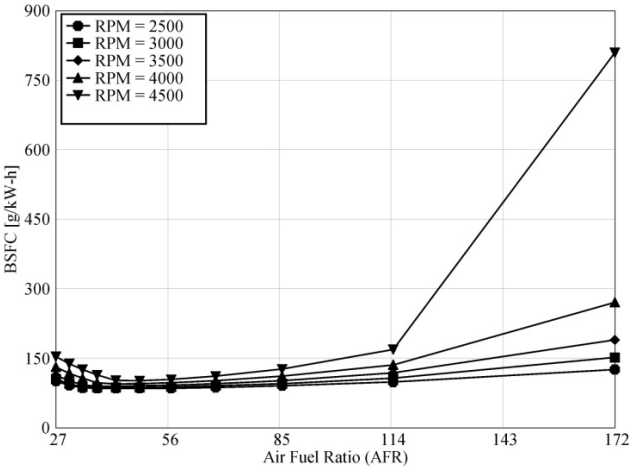

Fig. 6. Variation of brake specific fuel consumption with air fuel ratio for different engine speed

Figure 7 shows how the AFR can affect the maximum temperature inside the cylinder. In general, lower temperatures are required due to the reduction of pollutants. It is clearly demonstrated how the increase in the AFR can decrease the maximum cylinder temperature with a severe steeped curve. But for rich mixtures, the maximum cylinder temperature drops down with a linear manner. The effect of the engine speed on the relationship between maximum cylinder temperatures with AFR seems to be minor. At rich operating conditions (AFR= 27.464, ϕ =1.2) and a speed of 3000 rpm, a maximum cylinder temperature of 2767 *K* was recorded. This temperature dropped down to 1345 *K* at AFR of 171.65 (ϕ =0.2). This lower temperature inhibits the formation of NO_x pollutants. In fact this feature is one of the major motivations toward hydrogen fuel.

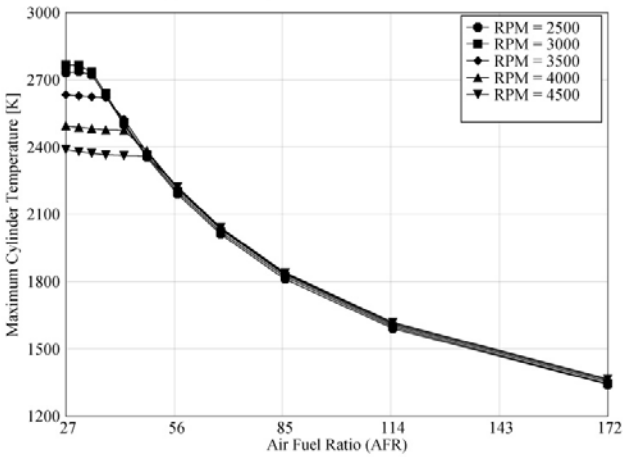

Fig. 7 Variation of maximum cylinder temperature with air fuel ratio

B. Instantaneous Behaviour on Crank Angle

The intake port and exhaust port pressures in terms of crank angle are shown in Figures 8 and 9 respectively. The instantaneous behavior is at the 12th cycle for wide open throttle (WOT) and stoichiometric operation. These figures (Fig. 8 and 9) are very important to investigate the backfire or pre-ignition occurrence in details. However, for the present case there is neither backfire nor pre-ignition and this is the case of normal combustion and shows typical results of pressure variation. The crank angle axis is divided into four parts to indicate the four strokes which take two cycles (720 degrees). The pressure seems to be a series of pulses. Each pulse is approximately sinusoidal in shape. The complexity of the phenomena that occur is apparent. Back flow from the cylinder into the intake manifold can be recognized during the early part of the intake process until the cylinder pressure falls below the manifold pressure. This happens within about 40 crank angle degrees and stops when the angle crank reaches 400 degree from the life cycle. Backflow also occur early in the compression stroke before the inlet valve closed due to rising cylinder pressure. The amplitude of the pressure fluctuations increases substantially with increasing engine speed. From Fig. 8, the maximum intake pressure was recorded 1.1 bar at speed 4500 rpm during the compression stroke, while it was 1.093 bar at speed of 2500 rpm. At the intake stroke, when high intake vacuum is occurred, the flow is continuously inward and flow pulsation is small. For high speed, larger pulses can be seen. At high speeds more fuel is required and consequently more vacuum in the intake port. A vacuum of 0.792 bar was calculated in 4500 rpm compared with 0.925 bar at 2500 rpm.

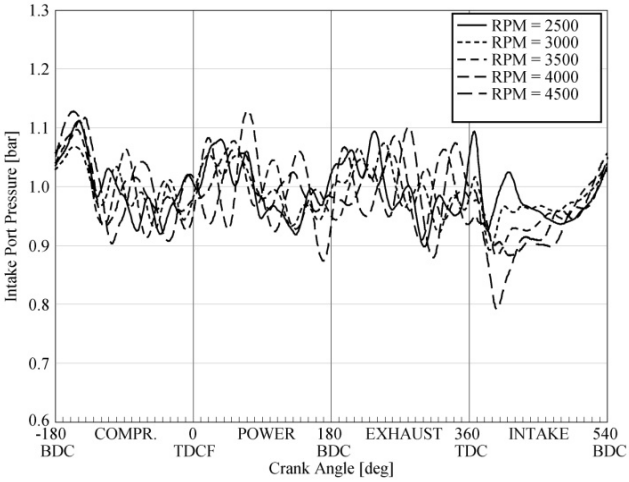

Fig. 8. Instantaneous intake port pressure distributions with crank angle for different speed

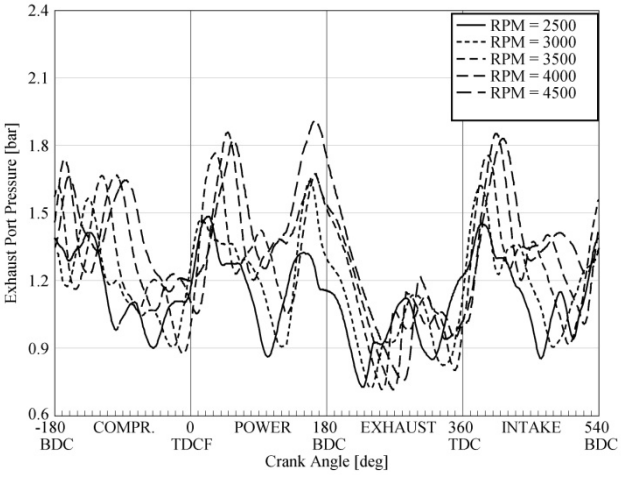

Fig. 9. Instantaneous exhaust port pressure distributions with crank angle for various engine speeds

The gas dynamic effects play a very important rule here. It distorts the exhaust flow which is shown in Fig. 9. The rise of the pressure at the end of the exhaust stroke can lead to reverse flow into the cylinder past the exhaust valve; however, the high vacuum in the beginning of the first stroke is highly desired to banish the burnt gases out of the cylinder. At speed of 3000 rpm, a maximum pressure of 1.64 bar and maximum vacuum of 0.72 bar were recorded. The response of fluctuation of the amplitude to the engine speed in case of exhaust pressure seems to be less than the intake pressure. But the fluctuation is also increasing with the increase of the engine speed.

Figure 10 illustrates the behavior of the cylinder pressure at the last cycle (12th cycle) for WOT and stoichiometric operation conditions. The behavior of the pressure follows the combustion phenomenon that occurs. The effect of the rotational speed on the instantaneous behavior of the cylinder pressure is minor. This curve can be divided into three parts for discussion purpose. The first part corresponds the flame development period which consumes about 5% of the air fuel mixture. Very little pressure rise is noticeable and little or no

useful work is produced. The second part corresponds the flame propagation period which consumes about 90% of the mixture. During this time, pressure in the cylinder is greatly increased, providing the force to produce work in the expansion stroke. The third part corresponds to flame termination period which consumes about the rest of the mixture (5%). In general this behavior is like the behavior of the traditional gasoline fuel, however, it is necessary to keep in mind that during the hydrogen combustion, the flame velocity is rapid and the main changes of cylinder pressure (the second part) occur in a shorter time.

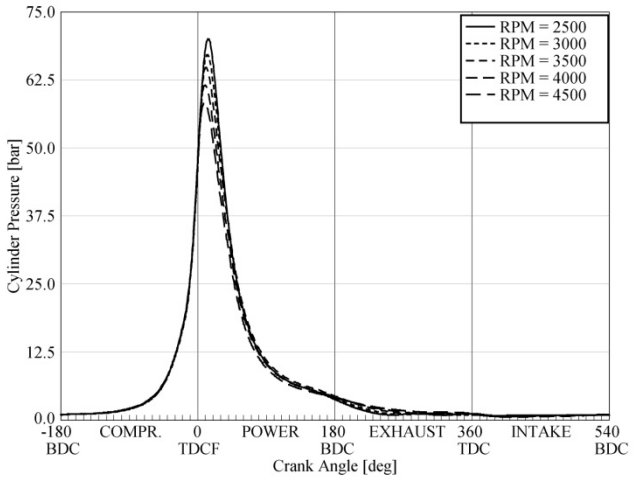

Fig. 10. Instantaneous cylinder pressure distributions with crank angle for various engine speed

IV. CONCLUSIONS

The present study considered the performance characteristics of a four cylinders hydrogen fueled internal combustion engine with hydrogen being injected directly in the cylinder. The following conclusions are drawn:

(i) At very lean conditions with low engine speeds, acceptable *BMEP* can be reached, while it is unacceptable for higher speeds. Lean operation leads to small values of *BMEP* compared with rich conditions.

(ii) Maximum brake thermal efficiency can be reached at mixture composition in the range of (ϕ = 0.9 to 0.8) and it decreases dramatically at leaner conditions.

(iii) The desired minimum *BSFC* occurs within a mixture composition range of (ϕ = 0.7 to 0.9). The operation with very lean condition (ϕ <0.2) and high engine speeds (>4500) consumes unacceptable amounts of fuel.

(iv) Lean operation conditions results in lower maximum cylinder temperature. A reduction of around 1400*K* can be gained if the engine works properly at (ϕ <0.2) instead of stoichiometric operation.

(v) Hydrogen combustion results in moderate pressures in the cylinder. This reduces the compactness required in the construction of the engine. But, if abnormal combustion like pre-ignition or backfire happens, higher pressures may destroy the connecting rod and piston rings. Therefore, much care should be paid for this point.

ACKNOWLEDGMENT

The authors would like to express their deep gratitude to Universiti Malaysia Pahang (UMP) for provided the laboratory facilities and financial support.

REFERENCES

[1] Suwanchotchoung, N. 2003. Performance of a spark ignition dual-fueled engine using split-injection timing. Ph.D. thesis, Vanderbilt University, Mechanical Engineering.

[2] COD (College of the Desert). 2001. Hydrogen fuel cell engines and related technologies, module 3: Hydrogen use in internal combustion engines. Rev. 0, pp. 1-29.

[3] White, C.M., R.R. Steeper and A.E. Lutz. 2006. The hydrogen-fueled internal combustion engine: a technical review. Int. J. Hydrogen Energy, 31(10):1292–1305.

[4] Mohammadi A, Shioji M, Nakai Y, Ishikura W, Tabo E. Performance and combustion characteristics of a direct injection SI hydrogen engine. Int J Hydrogen Energy 2007; 32:296-304.

[5] Guo LS, Lu HB, Li JD. A hydrogen injection system with solenoid valves for a four cylinder hydrogen-fuelled engine. Int J Hydrogen Energy 1999; 24:377-382.

[6] Verhelst S. A Study of the Combustion in Hydrogen-Fuelled Internal Combustion Engines. Ph.D. Thesis, Ghent University - UGent, Engineering, Mechanical; 2005.

[7] Tsujimura T, Mikami A, Achiha N. A Study of Direct Injection Diesel Engine Fueled with Hydrogen. SAE paper 2003; 2003-01-0761.

[8] Kim YY, Lee JT, Caton JA. The development of a dual-Injection hydrogen-fueled engine with high power and high efficiency. Journal of Engineering for Gas Turbines and Power, ASME 2006; 128:203-212.

[9] Rottengruber, H., M. Berckmüller, G. Elsässer, N. Brehm and C. Schwarz. 2004. Direct-injection hydrogen SI-engine operation strategy and power density potentials. SAE Paper No. 2004-01-2927.